EINDHOVEN UNIVERSITY OF TECHNOLOGY

Adhesion of electrolessly deposited Ni(P) layers on alumina ceramic II. Interface characterization

Citation for published version (APA):
Severin, J. W., Hokke, R., Wel, van der, H., & With, de, G. (1994). Adhesion of electrolessly deposited Ni(P) layers on alumina ceramic II. Interface characterization. *Journal of Applied Physics*, *75*(7), 3414-3422. https://doi.org/10.1063/1.356101

DOI:
10.1063/1.356101

Document status and date:
Published: 01/01/1994

Document Version:
Publisher's PDF, also known as Version of Record (includes final page, issue and volume numbers)

Please check the document version of this publication:

• A submitted manuscript is the version of the article upon submission and before peer-review. There can be important differences between the submitted version and the official published version of record. People interested in the research are advised to contact the author for the final version of the publication, or visit the DOI to the publisher's website.
• The final author version and the galley proof are versions of the publication after peer review.
• The final published version features the final layout of the paper including the volume, issue and page numbers.

Link to publication

General rights
Copyright and moral rights for the publications made accessible in the public portal are retained by the authors and/or other copyright owners and it is a condition of accessing publications that users recognise and abide by the legal requirements associated with these rights.

• Users may download and print one copy of any publication from the public portal for the purpose of private study or research.
• You may not further distribute the material or use it for any profit-making activity or commercial gain
• You may freely distribute the URL identifying the publication in the public portal.

If the publication is distributed under the terms of Article 25fa of the Dutch Copyright Act, indicated by the "Taverne" license above, please follow below link for the End User Agreement:

www.tue.nl/taverne

Take down policy
If you believe that this document breaches copyright please contact us at:

openaccess@tue.nl

providing details and we will investigate your claim.

Download date: 16. Nov. 2023

Adhesion of electrolessly deposited Ni(P) layers on alumina ceramic. II. Interface characterization

J. W. Severin, R. Hokke, H. van der Wel, and G. de With
Philips Research Laboratories, P.O. Box 80 000, 5600 JA Eindhoven, The Netherlands

(Received 3 September 1993; accepted for publication 29 November 1993)

The interface microstructure and interface chemistry of electrolessly deposited Ni(P) on alumina ceramics is studied in order to obtain insight into the influence of molecular interactions upon the adhesion. Detailed static secondary-ion-mass spectrometry, x-ray photoelectron spectroscopy, Auger electron spectroscopy, and transmission electron microscopy (TEM) analyses have been carried out with samples with various roughnesses, of which the mechanical analyses are described in the companion article. TEM cross-section micrographs showed a close contact between the two phases on a nanometer scale for all sample types. In addition, a 1–2-nm-thick interfacial layer was observed. This layer consists of nucleation material and compounds from the metallization solution. Fracture surface analyses showed that fracture takes place through this layer, which is therefore considered to be the weak boundary layer in this system. The presence of this weak boundary layer explains the importance of substrate surface roughness and mechanical interlocking for the fracture energy.

I. INTRODUCTION

The general aim of this adhesion study is described in the companion article,[1] where also a detailed mechanical analysis using various adhesion measurements, is presented. In this article the interface microstructure and interface chemistry are analyzed in order to obtain an interpretation for the previously measured macroscopic adhesion properties in terms of interfacial bonding on a molecular scale. The interface structure is analysed on micrometer and nanometer scale with transmission electron microscopy (TEM). For the analysis of the interface chemical composition, static secondary-ion-mass spectrometry (static SIMS), x-ray photoelectron spectroscopy (XPS), and Auger electron spectroscopy (AES) are used. Static SIMS is capable of determining the occurrence of organic structures at a submonolayer coverage. With AES the elemental composition of a surface can be quantitatively analyzed. With XPS inorganic structures and valencies are quantitatively measured at submonolayer coverage.

II. EXPERIMENTAL PROCEDURES

In this section the experimental procedures are described for the TEM, AES, XPS, and static SIMS interface analyses. The procedures followed for the sample preparation and the materials and solutions used are described in Ref. 1. The terms glycine-type Ni(P) and acetate-type Ni(P) refer to two different bath compositions used for the electroless deposition of the Ni(P) layers. Similarly, rough-type and smooth-type substrates denote two different substrate types.

A. Interface structure: Cross-section TEM micrographs

Cross-section TEM micrographs of the metal-ceramic interface were made using a Philips EM 400 transmission electron microscope at an electron energy of 120 keV. Samples were prepared by grinding, polishing, and ion milling as described in Ref. 2. Apart from TEM interface analyses of the adhesion strength test samples, samples with a smaller Ni layer thickness were also prepared for these TEM analyses with about 0.1 μm Ni(P) and without an electrodeposited Ni layer. Such a thinner metal layer facilitates the TEM sample preparation.

B. Interface chemistry: AES depth profiling

The AES spectra were obtained using a PHI 545 scanning auger microscope equipped with a cylindrical mirror analyzer. The background pressure was about 10^{-8} Pa. Sputtering was done using Ar^+ ions and a differentially pumped Ar sputter gun. A 3 keV ion beam was rastered over a 3×3 mm^2 area, the current density being 90 $\mu A/cm^2$, from which the sputtering rate was estimated to be about 13 nm/min. The 3 keV electron-beam diameter was about 5 μm and this beam was not rastered. The following Auger electrons were measured in this analysis, with the electron energy in eV (Ref. 3) between brackets: Sn *MNN* (430), Ag *MNN* (351), Pd *MNN* (330), Ni *LMM* (848), P *KLL* (120), S *KLL* (152), Al *LMM* (51), O *KLL* (505), C *KLL* (278). The analysis depth with this technique is 2–3 nm, mainly depending on the Auger electron energy.[2] The detection limit is about 0.5 at. %. For the AES measurements special samples with a thinner Ni layer were also prepared in order to minimize the roughening effect during sputtering. The same layer deposition procedure was followed as for the special TEM samples.

C. Interface chemistry: XPS analysis

Glycine-type Ni(P) layers were peeled from the smooth-type alumina substrates in a glovebox filled with purified N_2. The H_2O and O_2 contents in this atmosphere were <0.1 and 2.5 ppm, respectively, although it should be noted that the concentrations of these contaminants may be considerably higher in the vicinity of the rubber gloves.

 0021-8979/94/75(7)/3414/9/$6.00 © 1994 American Institute of Physics

Downloaded 23 Oct 2007 to 131.155.151.66. Redistribution subject to AIP license or copyright, see http://jap.aip.org/jap/copyright.jsp

TABLE I. Atom concentrations on the Ni(P) and the Al_2O_3 fracture surfaces of a sample with glycine-type Ni(P) on a smooth-type substrate. −20 nm: after 20 nm sputtering; box: after sputtering a subsequent transfer and stay in the glovebox for 30 minutes. Dashes indicate that no measurement was made.

Surface	C 1*s*	O 1*s*	Ni 2*p*3	Sn 3*d*5	Al 2*p*	P 2*p*	F 1*s*	Ag 3*d*5
Al_2O_3	13	52	4	0.2	28	1.3	0.6	—
$Al_2O_3^{-20\ nm}$	4	59	1.3	<0.1	35	<0.1	—	<0.1
Ni(P)[a]	27	23	40	0.4	—	9	—	0.5
$Ni(P)^{-20\ nm}$	8	4	79	0.1	<0.1	7	—	<0.1
$Ni(P)^{box}$	33	19	41	—	—	7	—	—

[a]An additional amount of about 1% N is detected at the Ni(P) surface.

From the glovebox the samples were transferred to the vacuum of the XPS apparatus in a vacuum-tight container.

The XPS measurements were done on a PHI 5400 apparatus equipped with a hemispherical analyzer, using Mg*K*α radiation (1253.6 eV) and an emission voltage of 13.5 keV. The background pressure was lower than 10^{-7} Pa. The analyzer was positioned at an angle of 45° relative to the substrate surface. A depth profile was made by alternatingly measuring and sputtering with 3 kV Ar^+ ions with a rate of 0.7 nm/min. By rastering the sputter beam, a crater of 7×7 mm^2 size is formed. The information depth is about 3 nm, which corresponds to 10–15 atomic layers. The spot size is about 2 mm^2. Overview spectra, multiscan detail measurements, and depth profiles were made. For the depth profiles, the intensities of the same peaks as those listed in Table I were followed. The exact peak positions (Table II) are measured using curve fitting. The relative concentrations (Table I) are calculated from the measured peak areas, assuming a homogeneous surface composition, both in depth and laterally. For this calculation Perkin-Elmer software is used (ESCA series model 8503A version V4.0 Rev. B 19-02-'91). The dependence of information depth upon kinetic energy of the measured photoelectrons is taken into account in the sensitivity factors in this software.

D. Interface chemistry: Static SIMS analysis

The chemical composition of the outermost monolayers of the nickel and alumina fracture surfaces was analyzed with static SIMS. After fracture, the nickel and alumina surfaces were introduced into the vacuum of the apparatus as quickly as possible, that is within a few minutes. During the measurements, ions were generated from these materials by bombardment of the surface with a primary beam of 10 keV Ar^+ ions of low ion dose, 10^{12} ions/cm^2. The spot diameter of the primary ion beam was approximately 50 μm. The secondary ions were accelerated to 2 keV and mass separated in a Reflectron-type time-of-flight mass analyzer described elsewhere.[4] Under these conditions the SIMS instrument operates within the static limit, i.e., the probability that an ion will hit a previously bombarded area is negligible. The analysis depth of this technique is of the order of a few monolayers (about 1 nm), its sensitivity is in the range of ppm of a monolayer. More details of the equipment and measuring conditions

TABLE II. Assignment of exact peak positions to chemical environment of the same sample as measured in Table I.

Element	Position (eV)	Rel. amount (%)	Environment
Ni(P) surface			
C	284.8	80	-C-H
	286.4	10	-C-O
	288.5	10	-O-C=O
O	532.8	25	-O-C
	531.1	75	PO_4, $Ni(OH)_2$ or Ni_2O_3
Sn	486.6	100	SnO_2 or SnO
P	132.3	25	$-P^{5+}$ ($-PO_4$)
	129.5	75	$-P^-$ (NiP)
Ni	852.2	70	Ni^0 metallic Ni
	853.2	10	Ni^{1+} (NiP)
	855.2	8	Ni^{2+} [$Ni(OH)_2$]
	857.0	12	Ni^{3+} ($NiPO_4$)
Al_2O_3 surface			
C	284.8	85	-C-H
	286.5	15	-C-O
O	533.2	7	-O-C
	531.0	93	Al_2O_3
Sn	487.6	100	SnF_4 or SnF_2
P	134.2	40	$-PO_3$
	132.5	60	P^{5+}, (PO_4)
Ni	851.7	15	Ni^0 (metallic Ni)
	852.6	10	Ni^{1+} (NiP)
	854.9	60	Ni^{2+} [$Ni(OH_2)$]
	857.7	15	Ni^{3+} ($NiPO_4$)
Al	73.8	100	Al_2O_3

are given in Ref. 4. The ratio of the integrated signal intensity of a peak characteristic of a surface compound and the signal intensity of a peak characteristic for the substrate (e.g., Ni^+, Al^+, AlO^-, NiO_2H^-), provides a relative measure of the surface coverage. These substrate signals can be used as reference intensities for the surface coverage because they originate from the outer 0–5 monolayers of the surface, whereas the organic molecules are in the first monolayer. A linear relationship between the relative static SIMS intensities and the absolute coverage has been established by van der Wel *et al.*[5] The mass resolution $m/\Delta m$ of the spectra is high enough (3000–5000 in the mass range 20–150 u) to distinguish peaks from metal ions from those of hydrocarbon ions of the same nominal mass.

III. RESULTS

A. Interface structure

1. Cross-section TEM

The cross-section TEM micrographs of the interfaces between both types of Ni(P) and the 96% and 99.5% alumina substrates are very similar. As a typical example, the micrograph of a sample with the rough-type substrate and acetate-type Ni(P) is shown in Fig. 1(a). Between both phases a layer of 1–2 nm thickness with an amor-

Downloaded 23 Oct 2007 to 131.155.151.66. Redistribution subject to AIP license or copyright, see http://jap.aip.org/jap/copyright.jsp

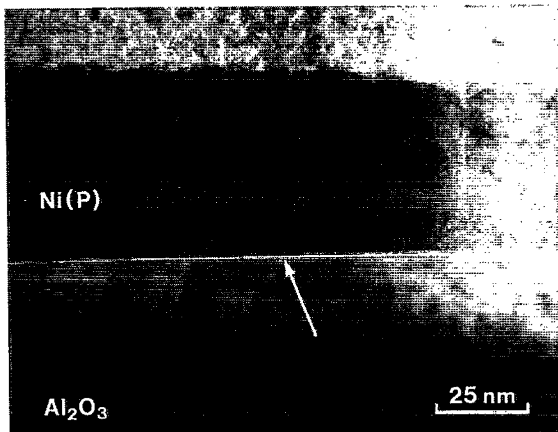

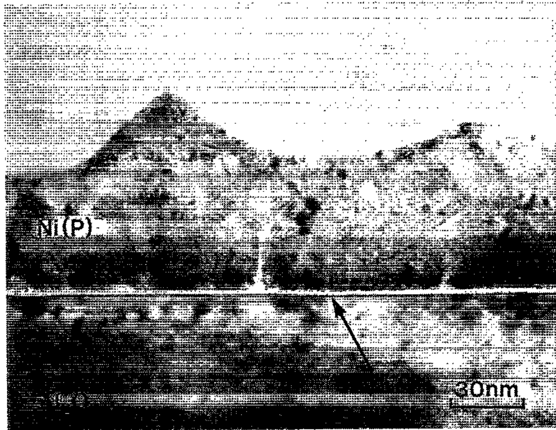

FIG. 1. Cross-section TEM micrographs of Ni(P) alumina interfaces: (a) sample with rough-type alumina and acetate-type Ni(P); (b) same sample type heated for 1 h at 160 °C.

phous structure is observed. Good interfacial contact is observed on all micrographs, no voids or interface gaps are observed within the resolution of about 0.5 nm. The structure of the material close to the interface can also be observed. On the micrographs the diffraction lines of the crystalline alumina grains are visible. In addition, a branching structure of Ni(P) columns indicates the coalescence of the initially formed small primary particles to fewer, broader columns during the growth process. The micrographs show that the Ni(P) layer thickness of these samples is of the order of 50–100 nm.

Figure 1(b) shows a TEM micrograph for the same sample type but for a sample that was used for the strength measurements. The same interface layer is observed. The structure of the Ni(P) material is quite different, though. Small crystalline particles are formed in the amorphous Ni(P) layer. The column structure has almost completely disappeared. This is probably due to the fact that this sample has been heated for 1 h at 160 °C for bonding the pull stud, as for all other adhesion strength test samples. However, according to Riedel,[6] crystallization of the amorphous Ni(P) deposit starts only at about 260 °C, as analyzed by x-ray diffraction. This apparent discrepancy may be explained by the fact that with TEM smaller crystals

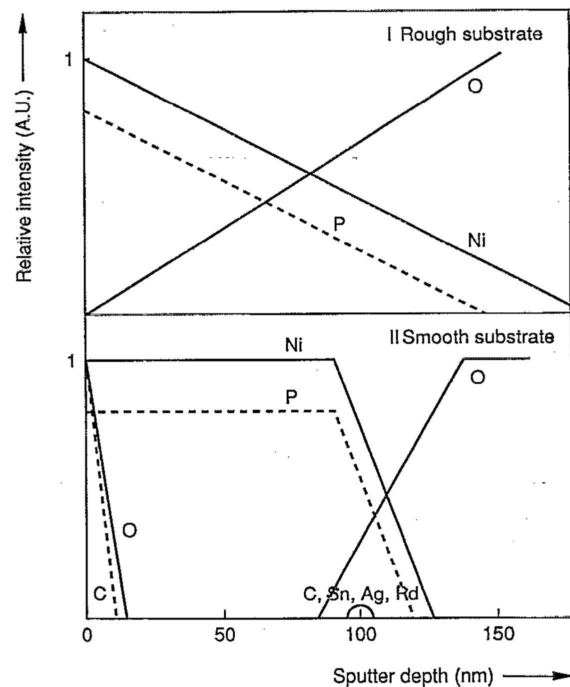

FIG. 2. Schematic representation of Auger depth profiles for rough- and smooth-type alumina substrates. For the relative intensity scale the Auger peak heights were used.

and thus an earlier stage of crystallization can be detected than with x-ray diffraction.

B. Chemical interface analysis

1. Auger electron spectroscopic depth profiling

The depth profiles obtained with AES from Ni(P) layers on the rough-type substrates are very different from those obtained from metal layers on smooth-type substrates (see the schematic representation in Fig. 2). In the depth profiles made from samples with rough substrates a gradual decrease in the intensity of signals from the metal layer is observed along with a gradual increase in intensity of the oxygen signal from the substrate. Due to this poor depth resolution, no signals could be measured of elements that are known to be present at the interface (e.g., Sn, Ag, Pd) in monolayer amounts.

From the samples with the smooth substrates the transition from layer to substrate can be distinguished better in the depth profiles. The elements Sn, Ag, and Pd which are used in the nucleation procedure are detected in the region where the intensity of the Ni signal decreases and that of the O (from the substrate oxide) signal increases. In the same range and of a similar intensity a signal from C appears as the interface is reached and disappears when the interface is passed and the substrate is measured. In the Ni(P) layer no C or O are detected; however, the signals of these interface species are only slightly stronger than the noise. The first reason for this is again the surface roughness and variation in layer thickness. The second reason is the relatively large noise due the short measuring time of 5 min used in these experiments. This measuring time is kept

Downloaded 23 Oct 2007 to 131.155.151.66. Redistribution subject to AIP license or copyright, see http://jap.aip.org/jap/copyright.jsp

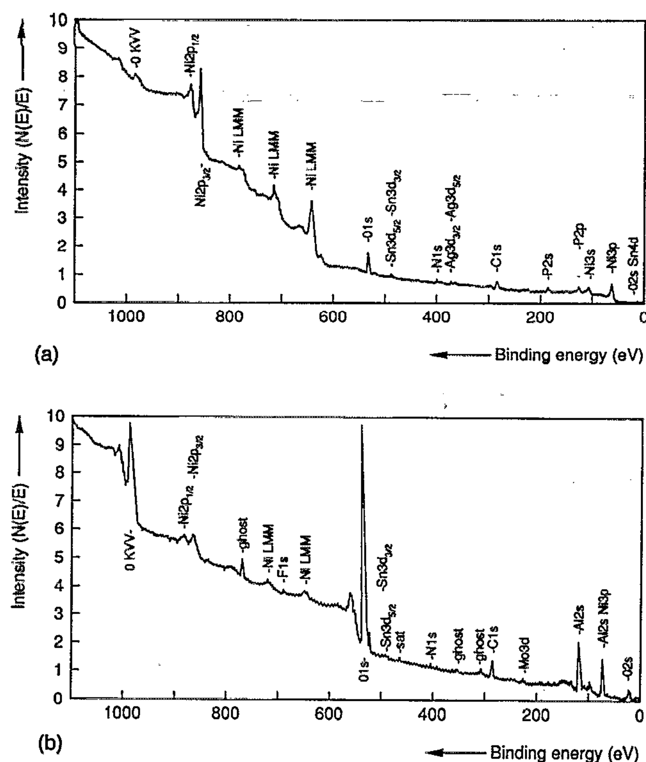

FIG. 3. (a) XPS overview spectrum of Ni(P) fracture surface; (b) XPS overview spectrum of Al_2O_3 fracture surface.

short in order to avoid interference by carbon contamination from the vacuum equipment. In a spectrum that was recorded in 5 min halfway through the metal layer, no carbon signal is observed, which means that contamination did not influence this measurement. As far as possible under these conditions, no differences are observed regarding the interfacial carbon between the Ni(P) deposited from the acetate-containing solution and the glycine-containing solution.

C. XPS fracture surface analysis

The XPS overview spectra, recorded from both fracture surfaces of a sample with glycine-type Ni(P) and a smooth-type substrate, are shown in Figs. 3(a) and 3(b), respectively. The peaks indicated by a "ghost" are due to instrumental effects (presence of weak lines other than Mg$K\alpha$ in the primary x-ray beam due to erosion of the Mg layer on the Cu anode). In Table I the atom concentrations, calculated from the peak areas in the multiscan detail measurements,[7] are listed. Relative accuracies of the values listed in Table I are estimated to be within 10%, except for the values which are close to the detection limit, which is about 0.1% for the elements reported here.

In Table II the assignment is given of exact peak positions to chemical environment (molecules, ions or compounds) of the same sample as in Table I. Reference data are used from Ref. 8.

These XPS measurements show that 80% of the Ni in the outer 3 nm of the Ni(P) fracture surface is metallic or intermetallic Ni. The other 20% is oxidized and consists of phosphate, hydroxide, or oxide. As a first approximation, this would correspond to an oxidized layer with an average thickness of 0.6 nm, or two atom layers. For the calculation of the relative amounts listed here, a homogeneous distribution of the various species over the analysis depth is assumed; however, the signal intensity of outer surface atoms is higher than those at about 3 nm below the surface. Since it is reasonable to assume that the oxide is present in the outermost surface of the Ni(P) layer, it is probably even less than corresponding to a layer with an average thickness of 0.6 nm, or in other words, less than two monolayers. The depth profiles, which are not shown here, reveal that most of the oxide is removed after 1.4 nm sputtering. After exposing the sputtered surface to the same procedure as used during the sample preparation (transfer in vessel and stay in glovebox), the same amounts of carbon and oxygen are found again on this surface (see Table I). This means that both the carbon and the oxygen that are detected on the fresh fracture surface may be completely or partly due to handling.

The amounts of carbon remaining on the Ni(P) and alumina fracture surfaces after 20 nm sputtering (8% and 4%, respectively) are rather high. The alumina ceramic certainly does not contain carbon in these amounts and the previously described AES measurements showed that the Ni(P) layer does not contain carbon either. A possible explanation can be found in the "shadow effect," frequently encountered on rough surfaces. The sputter beam is positioned at an angle of 54° to the surface and the analysis beam is at an angle of 40° to the sputter beam. Therefore, both beams do not apply to the same projections on a rough surface. Other phenomena which can increase the apparent width of a rough interface are redeposition of sputtered material and local variations of the sputter rate owing to the varying angle of the rough surface with the sputter beam.

The amount of nitrogen detected on the Ni(P) fracture surface is very small, of the order of 1%. This corresponds to 0.1 monolayer at most (order 10^{14} atoms N/cm^2). However, as part of an organic molecule, this small nitrogen coverage may be due to a close packing of glycine molecules on the surface, within the large uncertainty margin. The O-C=O coverage measured on this surface is in agreement with this assignment. Both species might, however, also originate from the surface contamination. Sn from the surface nucleation is detected both on the metal and the ceramic side of the interface. Pd is not detected on either side with XPS, indicating that the amount present at the interface must be less than about 0.1%. Fluorine, probably originating from the HF etching step, is present on ceramic, and at most amounts to 5% of a monolayer. It is not probable that the Ni and P which are detected on the ceramic surface are present as macroscopic particles. First, after sputtering of only 20 nm, the signal intensity of both species decreased more than threefold. Second, the smooth substrates used for this experiment do not give rise to remaining Ni(P) particles after peeling, as confirmed by the SEM/EDX analyses.[1] Third, the Ni ions are predominantly in the +2 and +3 oxidized state, in

Downloaded 23 Oct 2007 to 131.155.151.66. Redistribution subject to AIP license or copyright, see http://jap.aip.org/jap/copyright.jsp

TABLE III. Listing of main ions observed in the static SIMS measurements, in order of decreasing intensity. C_xH_y fragments originate from aliphatic hydrocarbons with $(x,y)=(1,3)$, (2,3), (2,5), (3,3), (3,5), (3,7), etc.

Rough-type substrate, acetate-type Ni(P)
Al_2O_3
+:Al, Ni, Na, C_xH_y, acetate, (K, Si, Mg)
−:O, HO, H, F, HCO_2, SiO_2, AlO, PO_2, C_2H, PO_3, Cl, CH_3CO_2 (acetate)
Ni
+:Ni, Na, Al, C_xH_y, CH_3CO (acetate)
−:O, OH, CH_3CO_2 (acetate), HCO_2, PO_2, PO_3, NiO_2H, NO_2, NO_3, Cl
Smooth-type substrate, acetate-type Ni(P)
Al_2O_3
+:Na, Al, Ni, C_xH_y, CH_3CO (acetate), SiOH, Si
−:O, OH, H, F, PO_2, PO_3, CH_3CO_2, AlO, HCO_2, Cl, SiO_2, SO_2, SO_3, NiO_2H
Ni
+:Ni, Na, C_xH_y, 43 CH_3CO, 43 C_xH_y
−:CH_3CO_2 (acetate), PO_3, PO_2, HCO_2, 46 C_2H, O_2, NiO_2H, Cl, SO_2, SO_3
Rough-type substrate, glycine-type Ni(P)
Al_2O_3
+:Al, Na, SiOH, CH_2NH_2 (glycine), Ni, CH_3CO (acetate), C_xH_y
−:O, OH, H, F, PO_2, PO_3, O_2, HCO_2, SiO_2, AlO, Cl, AlO_2, SO_2, SO_3
Ni
+:Ni, CH_2NH_2 (glycine), Na, C_xH_y, CH_3CO, C_xH_y
−:O, OH, H, Cl, PO_2, PO_3, HCO_2, NO_2, glycine, CH_3CO_2 (acetate), NiOH
Smooth-type substrate, glycine-type Ni(P)
Al_2O_3
+:Na, Al, CH_2NH_2 (glycine), C_xH_y, CH_3CO (acetate), Ni
−:O, OH, H, F, PO_2, PO_3, Cl, O_2, AlO, HCO_2, SO_2, SO_3, AlO_2, CH_3CO_2 (acetate), C_2H, SO_4, HSO_4
Ni
+:Ni, Na, CH_2 NH_2 (glycine), C_xH_y, CH_3CO, C_xH_y, CH_2N, C_xH_y, CH_3
−:O, OH, H, Cl, PO_2, PO_3, HCO_2, glycine, NO_2, CH_3CO_2 (acetate)
Blank Al_2O_3 after cleaning and etching
Rough-type substrate
+:Al, C_xH_y, Si, SiOH
−:H, O, OH, F, C_x $(x=1,2)$, C_xH $(x=1,2)$, AlO_x $(x=0-2)$, SiO_xH $(x=2,3)$
Smooth-type substrate
+:Al, Mg, C_xH_y, Si, SiOH
−:H, O, OH, F, C_x $(x=1,2)$, C_xH $(x=1,2)$, AlO_x $(x=0-2)$, SiO_xH $(x=2,3)$, Al_2O_4H, Al_2O_5H
$Al_3O_6H_2$

contrast to the solid Ni(P) material fracture surface. It is therefore probable that this material originates from small amounts of metallization solution which remain at the interface during metallization.

D. Static SIMS fracture surface analysis

In Table III a listing is given of the most important ions in the static SIMS spectra in decreasing order of signal intensity. The most intense signals originate from the substrate material on the Al_2O_3 side (Al^+ and AlO^-) and from the metal layer on the Ni(P) side (N^+ and NiO_2H^-). This means that no large amounts of contamination (less than several monolayers) are present on any of the samples. The positive and the negative ion static SIMS spectra of the blank surfaces of both types after cleaning and etching of the substrates are almost identical.

For all metallized samples, on the Al_2O_3 side ions are measured which originate from the Ni(P) layer, such as Ni^+, NiO_2H^-, PO_2^- and PO_3^-. For the samples with the rough-type substrates, these fragments may originate from small pieces of Ni(P) which remain on the substrate after delamination as observed with SEM.[1] However, for the smooth-type substrates this explanation cannot be valid, since no Ni(P) pieces remain on these substrates. This is discussed further in Sec. IV A, together with the XPS data. On the Ni(P) side of the interface no significant peaks of fragments characteristic of the smooth-type alumina substrate are found, such as Al^+ and AlO^-. The PO_2^- and PO_3^- that are measured in the negative ion spectra do not necessarily indicate that the Ni(P) is oxidized at the interface. It is to be expected that immediately after delamination a natural oxide layer is formed on the Ni(P) foils before they are introduced in the vacuum equipment.

Relatively strong peaks of Na^+ are often found on both sides of the interface of metallized samples. This means that Na^+ from the metallization solution remains at the interface, since it is not found on the blank samples after cleaning and etching. In the negative ion spectra of the ceramic surfaces F^- is one of the major peaks. It is also found on the blank alumina surfaces, which are cleaned

Downloaded 23 Oct 2007 to 131.155.151.66. Redistribution subject to AIP license or copyright, see http://jap.aip.org/jap/copyright.jsp

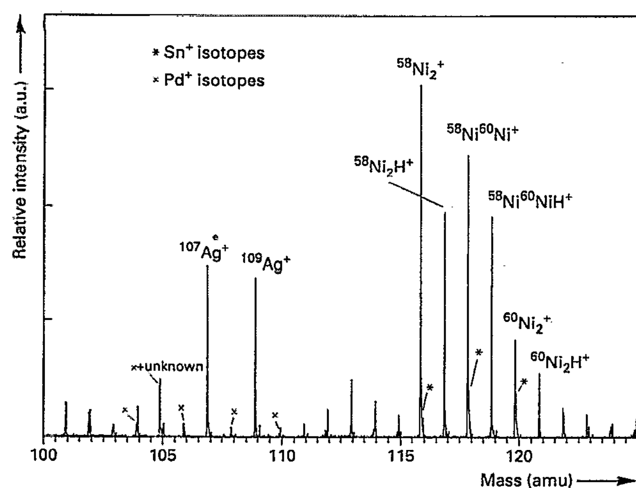

FIG. 4. Positive ion static SIMS spectrum in the mass range of the activator elements of the Ni(P) fracture surface of a sample with glycine-type Ni(P) and a smooth-type substrate. A linear intensity scale is used in the static SIMS spectra.

and etched in a HF solution. The F^- ions are therefore assumed to originate from this step. However, due to the high ionization probability of Na and F it cannot be concluded from the relatively high intensities that Na and F are major interface constituents.

The activator elements Sn, Ag, and Pd, are detected in small amounts (not listed in Table III, see Fig. 4) on the Ni(P) side of the interfaces. The Ag signal is stronger than the other ones. On the Al_2O_3 side only a weak signal of Sn is observed. It is therefore concluded that most of the activator material remains on the Ni side when fracture takes place.

Fragment ions originating from acetate and glycine are found in the spectra with considerable intensity, on both the Ni(P) and the alumina fracture surfaces. The relative intensities of fragments of these compounds are listed in Tables IV–VII.

Due to higher peaks from contamination in the positive ion spectra (see Table III), the presence of acetate and glycine can be analysed more accurately from the negative ion spectra. Peaks from glycine at the mass/charge (m/z) ratio 74 ($H_2NCH_2COO^-$) are measured only on samples that are prepared from the glycine-containing metallization solution, on both the Al_2O_3 and the Ni(P) side of the interface; see Tables IV and V, respectively. Both on the Ni(P) side and on the Al_2O_3 side most acetate (m/z 59, CH_3COO^-) is found for the samples that are prepared from the acetate-containing electroless solution. On the alumina side an increase of about 20 times is measured relative to the blank rough and smooth alumina substrates. However, on the glycine samples an increase in acetate coverage is also measured, relative to the blank alumina surfaces. This can be explained by the affinity of acetic acid present in the laboratory ambient, for the basic amino end groups of the glycine-covered samples.

Also in the positive ion spectra, glycine (m/z 30, $CH_2{=}NH_2$) is mainly found on the fracture surfaces of samples prepared with the glycine-containing electroless solution, both on the Ni(P) side and on the Al_2O_3 side. In fact, the intensity of $m/z\ 30^+$ is negligible on the other metallized and blank samples. The interpretation of the acetate coverage of the samples is hampered by the presence of organic contamination, which may give rise to the same fragments.

This influence of contamination is confirmed in a separate experiment for the glycine-type Ni(P) smooth-type alumina fracture surface. In this experiment the sample was peeled in vacuum in the mass spectrometer. On the Ni(P) and the Al_2O_3 sides no acetate, formiate, or hydrocarbon fragments could be found. However, after placing these fracture surfaces for a few minutes in air, static SIMS analyses show the same amounts of acetate, formiate, and hydrocarbons as those observed for the surfaces discussed in Tables III–VII. In Fig. 5 static SIMS spectra are shown from the glycine-type fracture surface before and after exposure to air. In the positive ion spectra, the peaks indicated with an asterisk originate from molecules which appeared after exposure of the peeled surface to air. In the negative ion spectra assignments are given of the new peaks.

TABLE IV. Static SIMS intensities of the negative ion spectra (relative to AlO^-, ×100%) of interface compounds on the Al_2O_3 fracture surfaces of the test samples and blank Al_2O_3 surfaces.

Al_2O_3	Ni(P)	$CH_3CO_2^-$ (59)	$H_2NCH_2CO_2^-$ (74)
Rough	glycine	32.1	9.6
Rough	acetate	76.8	···
Rough	blank	4.3	···
Smooth	glycine	37.3	17.7
Smooth	acetate	192	···
Smooth	blank	8.7	···

TABLE V. Static SIMS intensities of the negative ion spectra (relative to NiO_2H^-, ×100%) of interface compounds on the Ni(P) fracture surfaces of the test samples.

Al_2O_3	Ni(P)	$CH_3CO_2^-$ (59)	$H_2NCH_2CO_2^-$ (74)
Rough	glycine	145	193
Rough	acetate	529	···
Smooth	glycine	210	261
Smooth	acetate	679	···

TABLE VI. Static SIMS intensities of the positive ion spectra (relative to Al^+, ×100%) of interface compounds on the Al_2O_3 fracture surfaces of the test samples and blank Al_2O_3 surfaces.

Al_2O_3	Ni(P)	$CH_2NH_2^+$ (30)	CH_3CO^+ (43)	CH_3^+ (15)
Rough	glycine	6.7	2.9	1.4
Rough	acetate	0.1	2.5	2.1
Rough	blank	0.8	1.6	1.0
Smooth	glycine	15.1	6.9	3.0
Smooth	acetate	···	4.5	3.1
Smooth	blank	1.1	3.6	1.6

Downloaded 23 Oct 2007 to 131.155.151.66. Redistribution subject to AIP license or copyright, see http://jap.aip.org/jap/copyright.jsp

TABLE VII. Static SIMS intensities of the positive ion spectra (relative to Ni^+, ×100%) of interface compounds on the Ni(P) fracture surfaces of the test samples.

Al_2O_3	Ni(P)	$CH_2NH_2^+$ (30)	CH_3CO^+ (43)	CH_3^+ (15)
Rough	glycine	638.0	4.0	2.8
Rough	acetate	1.0	1.8	1.6
Smooth	glycine	43.3	5.2	3.8
Smooth	acetate	0.3	9.7	7.1

IV. DISCUSSION

A. Fracture path

The cross-sectional TEM micrographs show that an interfacial layer of 1–2 nm thickness is present for all the Ni(P) alumina samples investigated. In high-resolution TEM micrographs of a sputtered Ti layer on the same smooth-type alumina, a sharp transition from ceramic to metal is observed.[9] This means that the interfacial layer is not a characteristic feature of the substrate material, such as, e.g., a hydrolyzed surface layer. It must be concluded, therefore, that the interface layer is formed by deposition of Ni(P). Apart from this interfacial layer, with TEM a good interfacial contact was observed for all samples. With static SIMS and XPS it is shown that the outermost monolayers of the metal and ceramic fracture surfaces mainly consist of Ni(P) and alumina, respectively. Therefore, it is concluded that fracture takes place exactly through this interfacial layer which may therefore be regarded here as the weakest link in the chain. The nature, composition, and origin of this layer are thus of great importance for this investigation. An overview of the most important information on the composition of this interfacial layer from static SIMS, AES, and XPS is presented in Table VIII. For the sake of completeness, results of Rutherford backscattering spectrometry (RBS) analyses, which were not previously described, are added.

In the following discussion, a number of possible contributions to the composition of the interfacial layer are considered successively.

1. Activator material

The interfacial layer partly consists of activator material. XRF measurements have shown that the amount of activator material (Sn, Ag, and Pd) before deposition of Ni(P) is about a monolayer (of the order of 10^{19} metal atoms per m^2) with the present nucleation procedure.[10]

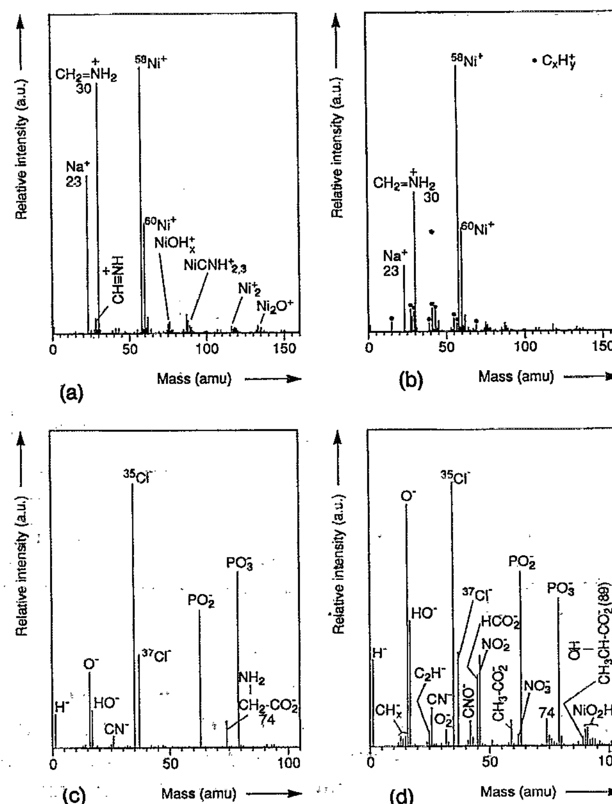

FIG. 5. Positive and negative ion static SIMS spectra of glycine Ni(P) surface (a) and (c) after debonding in vacuum and (b) and (d) after subsequent exposure to air (*B*,*D*). A linear intensity scale is used in the static SIMS spectra.

Also by AES depth profiling and XPS and static SIMS fracture surface analysis of Ni(P), these elements are detected at the interface; however, the amount of nucleation material is not enough to account for the whole layer thickness as observed with TEM.

2. Remaining compounds from metallization solution

It is possible that also a thin layer of solution remains at the interface during metallization. In fact, all of the compounds of the metallization solution can be recognized in the static SIMS spectra. The XPS measurements show that on the alumina fracture surface Ni is present which cannot be explained by the presence of remaining Ni(P) particles, since this Ni is for the greater part removed by sputtering only 20 nm. Moreover, the ratio of oxidized Ni

TABLE VIII. Overview of most important chemical analysis data on interfacial composition.

Technique	Constituents organic	Sn, Ag, Pd	F	N	Cl	Other
Static SIMS	glycine/acetate	Sn, Ag, Pd	F	N[a]	Cl	O, Ni, PO_2, PO_3
XPS	various C	Sn, Ag	F	N[a]	⋯	O, $Ni(OH)_2$, $NiPO_4$
AES[b]	C	Sn, Ag, Pd	⋯	⋯	⋯	⋯
RBS[c]		(Sn, Ag, Pd)	⋯	⋯	Cl	⋯

[a]Only for glycine-type Ni(P).
[b]Depth profile.
[c]Analyzed after nucleation, before Ni(P) deposition.

Downloaded 23 Oct 2007 to 131.155.151.66. Redistribution subject to AIP license or copyright, see http://jap.aip.org/jap/copyright.jsp

versus metallic or intermetallic Ni is greater on the alumina surface, compared to the Ni signals on the Ni(P) fracture surface. It is observed that the adhesion of Ni(P) on very smooth nonconducting substrates, such as float glass, is considerably increased after drying the sample when the first metal layer has been deposited. Even the slightest stress leads to cracking and buckling of the Ni(P) films during deposition and the film can be wiped off with a tissue in the wet state. Therefore, an intermediate drying step is often used after deposition of the first 0.1 μm when using smooth surfaces. Probably water is bonded to the oxide surface more strongly than the freshly deposited Ni(P) and capillarity or inclusion effects may play a role as well. After the water is evaporated, remaining components of the metallization solution may contribute to the formation of an interface layer. Due to the cracking and buckling effect described above, it is difficult to prepare samples of Ni(P) layers on perfectly smooth substrates, although the adhesion in the dry state may be acceptable.

3. Carbon at the interface

It is very probable that the carbon detected at the interface with AES originates from acetate or glycine detected at the interface with static SIMS. On the glycine-type Ni(P) and alumina fracture surfaces, after debonding in the vacuum of the static SIMS apparatus, hardly any other organic compounds (contaminations) are measured. Therefore, it is unlikely that the carbon signal in the AES spectra at the interface is caused by organic contaminations. In the case of glycine, N should also have been detected by AES, which was not the case. It is, however, possible that the N signal has remained below the detection level because only one N atom is present per two C atoms, and the signal due to C at the interface is already very weak.

B. Mechanism of adhesion

1. The contribution of mechanical interlocking

The mechanism of adhesion describes the type of intrinsic interfacial (chemical or mechanical) interactions. Most authors[11–16] who studied the adhesion of Ni(P) using 96% alumina, observed that the adhesion is strongly influenced by etching conditions and therefore conclude that the adhesion is determined by mechanical interlocking.[17]

Osaka *et al.*[15] concluded from experiments with electroless Cu using Ni(P) underlayers, that apart from mechanical interlocking, additional, interfacial phenomena also play a role in the adhesion. All these literature data are obtained by adhesion strength measurements only, which, as explained in Ref. 1, are insufficient for drawing conclusions about intrinsic interfacial interactions. The peel energy values for the rough-type substrates are about five times higher than those for the smooth substrates, as reported in Ref. 1. Since small pieces of Ni or Ni(P) remain between surface grains of the rough ceramic substrates and local deformations are observed on the metal fracture surfaces, it is concluded that mechanical interlocking forms the largest contribution to the intrinsic fracture energy for samples with the rough-type substrates. This interlocking model is illustrated by the cross-section optical micrograph in Ref. 1.

The influence of surface roughness on the adhesion is more complex than suggested by the simple model of rupture of penetrated parts of the film which remain in substrate pores. Oh, Cannon, and Ritchie[18] illustrated nicely how the interface microstructure influences the fracture energy with unaltered chemical interactions for thermocompressed copper foils on glass. By deliberately introducing small interfacial flaws, bridging ligaments were created behind the advancing crack front. The additional energy dissipation in these ligaments is larger than the original fracture energy. On rough-type substrates used in this study, fracture may take place similarly.

2. Van der Waals and other chemical interactions

For both the rough- and the smooth-type substrates it is observed that the moisture content of the atmosphere significantly influences the peel energy value. This cannot be explained by mechanical adhesion, only by chemical adhesion, including van der Waals interactions. Since the interfacial area increases along with the roughness during etching, chemical interactions may increase as well as mechanical interactions. Therefore, with the present results it can be concluded that for the rough-type substrates both mechanical and chemical interactions play a role in the adhesion. With the present data it is not possible to make a quantitative estimation of each contribution. For the smooth substrates no evidence is obtained that mechanical interactions play a role in the adhesion, since no metal remains on the ceramic fracture surface and on the metal fracture surface no local plastic deformations can be distinguished.

Since the fracture always takes place exactly along the interface, except for the interlocking sites on the rough substrates, it must be concluded that the chemical bonds in both the metal layer and the substrate are much stronger than at the interface. Therefore, it is probable that interfacial bonding is brought about by van der Waals interactions between the constituents of the amorphous interfacial layer shown in the TEM micrographs.

Van der Waals interactions amount to 0.5 J/m^2 maximally, but for the interfaces studied here this is probably less, due to the presence of organic and probably also inorganic molecules at the interface. Nevertheless, a peel energy of at least 7 J/m^2 is measured. This difference may be explained by the crack-tip plastic deformation processes described in Ref. 1. For the thermocompressed Ni alumina system fracture energies of about 150 J/m^2 were measured, while an intrinsic fracture energy of a few J/m^2 was calculated.[19] This implies that for that system the energy loss factor f_l (Sec. II) is of the order of 100.

V. CONCLUSIONS

This contribution clearly demonstrates the complexity of the adhesion of electroless Ni(P) to alumina ceramics. It has been shown that a fracture mechanical approach,

Downloaded 23 Oct 2007 to 131.155.151.66. Redistribution subject to AIP license or copyright, see http://jap.aip.org/jap/copyright.jsp

along with a thorough characterization of chemistry and structure of the interface, is required for obtaining insight in the adhesion.

By static SIMS measurements most of the components in the metallization solutions are found on the corresponding fracture surfaces for both sample types. This was also the case for the glycine and acetate complexing agents, which was the only significant difference between the spectra of the two sample types. Nucleation material is also found to be present on both the layer and the substrate fracture surfaces. In addition, by XPS it was shown that the interfacial layer cannot be completely explained by oxidation of Ni(P) at the interface during or after deposition.

The Ni(P) alumina interface structure, studied with cross-section TEM, was very different from that of most other metal-ceramic systems prepared by, for example, vacuum deposition of metal layers or by thermocompression of metal films on ceramics.[20] For such systems a sharp transition is generally observed between metal and ceramic, while for the Ni(P) alumina system, an interface layer with a thickness of 1–2 nm is observed for all samples. Fracture takes place at or in this layer. Apart from the interface layer, a close contact between layer and substrate is observed for all samples. Based on the fracture energy measurements and the TEM investigations, it is concluded that differences in adhesion strength of the various sample types cannot be accounted for by differences in interfacial structure at nanometer level.

ACKNOWLEDGMENTS

Gratitude is expressed to P. Oosting for Auger analyses, F. Vreugdenhil (CFT) for the XPS analyses, and J. Janssen (Components Roermond) for stimulating discussions.

[1] J. W. Severin, R. Hokke, and G. de With, J. Appl. Phys. **75**, 3402 (1994); J. W. Severin, Ph.D. thesis, Technical University of Eindhoven, 1993, available at Philips Research Laboratories, P.O. Box 80,000, 5600 JA, Eindhoven, The Netherlands.

[2] L. C. Feldman and J. W. Mayer, *Fundamentals of Surface and Thin Film Analysis* (Elsevier, New York, 1986).

[3] L. E. Davis, N. C. MacDonald, P. W. Palmberg, G. E. Riach, and R. E. Weber, *PHI Handbook of Auger Electron Spectroscopy* (Physical Electronics Division, Perkin-Elmer Corporation, Eden Prairie, MN, 1978).

[4] H. van der Wel, P. N. T. van Velzen, U. Jürgens, and A. Benninghoven, in *Analysis of Microelectronic Materials and Devices*, edited by M. Grasserbauer and H. W. Werner (Wiley, New York, 1991), Chap. 2, 10.

[5] H. van der Wel, J. Lub, P. N. T. van Velzen, and A. Benninghoven, Microchim. Acta (Wien) **2**, 3 (1990).

[6] W. Riedel, in *Funktionelle Chemische Vernicklung* (E. G. Leuze, Saulgau, 1989), p. 111.

[7] F. Vreugdenhil (private communication).

[8] K. S. Rajam, S. R. Rajagopalan, M. S. Hegde, and B. Viswanathan, Mater. Chem. Phys. **27**, 141 (1991); National Institute of Standards and Technology XPS data base version 1.0, October 1989, NIST, Gaithersburg, MD.

[9] J. W. Severin, R. Hokke, H. van der Wel, M. Johnson, and G. de With, J. Electrochem. Soc. **140**, 1611 (1993).

[10] J. W. Severin, R. Hokke, H. van der Wel, and G. de With, J. Electrochem. Soc. **140**, 682 (1993).

[11] H. Honma and S. Mizushima, Kinzoko Hyomen Gijutsu **33**, 380 (1982).

[12] T. Osaka, E. Nakajima, Y. Tamiya, and I. Koiwa, Kinzoko Hyomen Gijutsu **40**, 67 (1989).

[13] T. Osaka, Y. Tamiya, K. Naito, and K. Sakaguchi, J. Jpn. Inst. Printed Circuit **4**, 285 (1989).

[14] H. Honma and K. Kanemitsu, Plating and Surface Finishing **74**, 62 (1987).

[15] T. Osaka, Y. Tamiya, K. Naito, and K. Sakaguchi, J. Surf. Finish. Soc. Jpn. **40**, 835 (1989).

[16] M. Kamijo and N. Ayuzawa, Yamanashi-Ken, Kogyo Gijutsu Senta Kenkyu Hokoku, 1987, Vol. 1, p. 86 (research report of the Yamanashi Prefectural Industrial Technology Center).

[17] J. W. Severin and G. de With, J. Adhesion Sci. Technol. **7**, 115 (1992).

[18] T. S. Oh, R. M. Cannon, and R. O. Ritchie, Mater. Res. Soc. Symp. Proc. **130**, 219 (1989).

[19] H. F. Fischmeister, G. Elssner, B. Gibbesch, and W. Mader, Materials Research Society International Meeting on Advanced Materials 8, 1988, p. 227.

[20] M. Rühle and W. Mader, in *Designing Interfaces for Technological Applications*, edited by S. D. Peteves (Elsevier, London, 1989), p. 145.

Downloaded 23 Oct 2007 to 131.155.151.66. Redistribution subject to AIP license or copyright, see http://jap.aip.org/jap/copyright.jsp